European Journal of Physics

PAPER

Hitting a ball on a spring: a simple model for understanding decoherence with wavefunctions

IOP Publishing European Journal of Physics
Eur. J. Phys. **41** (2020) 025401 (25pp) https://doi.org/10.1088/1361-6404/ab4d10

Hitting a ball on a spring: a simple model for understanding decoherence with wavefunctions

Matthew C Schram[1,3] **and Eric J Heller**[2]

[1] Department of Physics, Massachusetts Institute of Technology, United States of America
[2] Department of Physics, Harvard University, United States of America

E-mail: schram@mit.edu and heller@physics.harvard.edu

Received 21 July 2019, revised 18 September 2019
Accepted for publication 11 October 2019
Published 16 January 2020

Abstract

The typical approach to studying decoherence begins by examining a combined system and interacting environment (termed bath), and then deriving a master equation to examine the behaviour of the density matrix after tracing over the bath, typically by invoking the Markovian approximation. This approach is quite successful for a large variety of systems however is frequently a non-intuitive picture that can mask the fundamental behaviour of the system. We examine here a simple model that captures the essence of decoherence and study it using the wavefunction picture, invoking the analytic concepts of the correspondence principle, the method of images, the phase jitter concept, and the scattering matrix formalism. We complement this with a numerical study using the split-operator FFT method, the forced harmonic oscillator method, and the thawed Gaussian approximation.

Supplementary material for this article is available online

Keywords: decoherence, semiclassics, wavefunctions

(Some figures may appear in colour only in the online journal)

1. Introduction

Quantum decoherence is the process by which a quantum state loses fundamental information via its interaction with the environment around it. This interaction is compelling for

[3] Current Address: Alivecor, Inc, 444 Castro Street 600, Mountain View, CA 94041, United States of America.

fundamental reasons of understanding the very nature of quantum mechanics, the measurement process, and the boundary between quantum and classical behaviour [1]. Moreover, the promise of quantum computation demands engineering qubits whose states remain entangled and self-coherent long enough to perform useful operations before environment-induced interactions degrade the qubits to become classical bits [2]. To specify a concrete example, coherence or decoherence is the fundamental difference between saying that a particle is simultaneously spin up and spin down, or that the particle is either spin up or spin down.

The standard approach approach to studying environmental decoherence involves placing the system in contact with a many-particle thermal 'bath.' Practically, this involves forming the density matrix from the initially separable system. The effective time evolution is described by tracing over the bath variables to obtain the reduced density matrix, which evolves under a master equation. This master equation generally involves a phenomenologically derived dissipative term, either derived from Markovian (i.e. memoryless [3]) dynamics or some other type of non-Markovian dynamics [4]. This approach has had great success in predicting certain types of phenomena, particularly when dealing with a stochastic, thermal bath [5]. Moreover, this decoherence scheme can naturally lead to so-called pointer states [6] emerging, which for appropriate dynamics can yield classical states. Indeed, this is one of the reasons [1] why this procedure has been used to study the measurement process.

However, this scheme can mask underlying behaviour by solely considering the dynamics of the system rather than the combined picture. In extreme cases it can reduce the problem to a heuristic process of trying to conjecture a master equation with minimal physical intuition. Instead of considering a collection of bath particles, we here consider one 'bath' particle interacting with the system (a similar sort of minimal heat bath model was studied by Ingold *et al* [7] in analysing anomalous specific heat in the Drude model of open quantum systems). Furthermore, instead of treating the bath as a thermal, statistical ensemble, we treat the 'bath' exactly as an initially zero temperature particle. We stay in the wavefunction picture as we analyse a free particle incident upon a harmonic oscillator to provide a clear characterisation of the decoherence the particle undergoes throughout this interaction. We study this model both analytically (using approximations in different physical regimes as well as deriving an exact solution) and numerically (using the split-operator FFT method, the forced harmonic oscillator approximation and the thawed Gaussian approximation).

For the model we present here, the initially uncoupled system particle becomes entangled with our 'bath' particle, which acts to measure the state of the system. Under appropriate parameters, the probabilistic excitation of the bath acts to reduce the system to classical (the recent work by Clarke [8] provides an excellent background in the quantum to classical transition and the interpretations surrounding measurement theory. Note that irreversible statistical transitions can be obtained from a purely classical standpoint; see, for instance, Kardar's work on the kinetic theory of gases [9]). We evolve the joint system's wavefunction in time, and alternately, average (i.e. trace) out the bath variables to get the behaviour of the system and average out the system variables to understand how the bath has measured the system (Gamble and Lindrer [5] give an explicit description of the combined product state between the system and bath and the subsequent trace operation). The purest notion of the degree of decoherence can be seen by considering the degradation of the off-diagonal elements of the density matrix to quantify how decohered the 'average' interaction has made the system [10].

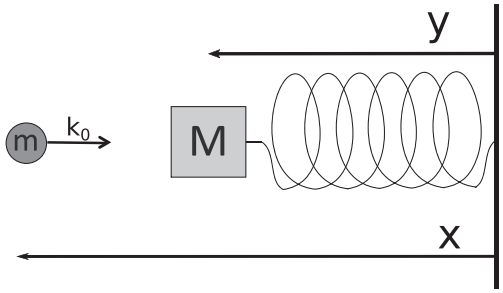

Figure 1. Classical scattering schematic—a free particle of mass m and momentum k_0 is incident upon a harmonic oscillator of mass M. x refers to the position of the free particle, while y refers to the position of the harmonic oscillator.

2. A simple decoherence model

A simple model which incorporates these features starts with the Hamiltonian of a free particle (the system, in decoherence terminology), represented by coordinates (p_x, x), originating from $x = -\infty$, moving towards a particle in a harmonic oscillator potential (the bath), represented by coordinates p_y, y, with a sharp wall-like potential between the two particles:

$$\hat{H} = \frac{p_x^2}{2m} + \frac{p_y^2}{2M} + \frac{1}{2}M\omega^2 y^2 + \lambda\Theta(x - y) \tag{1}$$

as shown in figure 1. To simplify the problem, we first make a coordinate transform to scale the mass of the harmonic oscillator to be identical to that of the free particle. This transformation takes the canonical momentum $p_y \rightarrow \sqrt{\frac{M}{m}}p_y$, which has a corresponding coordinate scaling of $y \rightarrow \sqrt{\frac{m}{M}}y$ to preserve the volume of phase space. This transformation yields

$$\hat{H} = \frac{p_x^2}{2m} + \frac{p_y^2}{2m} + \frac{1}{2}m\omega^2 y^2 + \lambda\Theta\left(x - \sqrt{\frac{m}{M}}y\right) \tag{2}$$

or, $\hat{H} = \hat{H}_0 + \hat{V}_I$ where $\hat{H}_0$ is the Hamiltonian of the two particles without interaction, and $\hat{V}_I = \lambda\Theta\left(x - \sqrt{\frac{m}{M}}y\right)$ is the interaction term.

Before solving this problem, first consider the one-coordinate version where we take the target $M \rightarrow \infty$ (turning the oscillator into a fixed wall), take $\lambda \rightarrow \infty$ and displace the target by distance a. The boundary conditions restrict the solution to this potential to be a superposition of an incoming wave and an outgoing wave such that $\psi(x = a) = 0$. Adding the conventional normalisation and taking $\hbar = 1$, our wavefunction [11] is

$$\begin{aligned}\psi_k(x) &= \frac{1}{2i}\sqrt{\frac{1}{\pi}}\left(e^{ik(x-a)} - e^{-ik(x-a)}\right) \\ &= \sqrt{\frac{1}{\pi}}\sin\left(k(x - a)\right)\end{aligned} \tag{3}$$

for $x < a$, and $\psi_k(x) = 0$ for $x > a$. The probability amplitude of the wavefunction is then

$$|\psi_k(x)|^2 = \frac{1}{2\pi}(1 - \cos\left(2k(x - a)\right)). \tag{4}$$

This yields interference with perfect contrast (there are zeros of the function where the wavefunction is completely extinguished), one of the tell-tale signs of quantum mechanical

coherence. In effect, with an infinite mass wall, the ability of the particle to 'measure' the collision of the scatterer is null due to the negligible transfer of energy or momentum. This is remains true even for noninfinite λ $\left(\text{provided that} \frac{p_x^2}{2m} < \lambda\right)$, or for other types of softer potentials; the only difference in these cases is a phase shift. As we will see, the effect of transforming the infinite mass hard wall into a finite mass particle is to cause the plane wave to bounce off a slanted wall, distorting the outgoing wave. We will see that, after averaging out the bath particle, the reduced wavefunction has the general form

$$|\psi_k(x)|^2 = \frac{1}{2\pi}(1 - |c_0|\cos(2k(x - a))), \tag{5}$$

where we will see that $|c_0|$ is the overlap of the ground state of the harmonic oscillator. Note that if one plots equation (5), one can still see the interference pattern, but this fringe contrast (the ratio of the difference between peaks and troughs of the function and the average of the function) is reduced according to $|c_0|$.

This toy model, which incorporates the behaviour we are looking for, is not quite as purely theoretical as one might assume. When studying neutron interferometry, the degree of recoil in the mirrors of the interferometer acts to reduce the interference contrast of the recombined neutron beam due to the mirrors 'measuring' the neutron and gaining information about its path. Instead of treating the mirror as a free particle as is done in the review of neutron interferometry by Greenberger [12], the mirror could instead be treated as a stiff, heavy oscillator in the framework we develop here.

3. Analytical approaches

We now look to develop approximate and exact solutions for this model in stages. We begin with examining the problem using classical-quantum analogues using the coherent states of quantum harmonic oscillators. We then look at an approximation of wavefunction reflection using the boundary condition that for an infinite strength wall, the wavefunction at $x = \sqrt{\frac{m}{M}}y$ must be zero. We then look at a phase jitter model where we approximate the scattering by averaging the simultaneous scattering over the probabilistic positions of the quantum harmonic oscillator. Finally, we explicitly solve the model using the formalism of scattering matrices. We then compare the results of these solutions to look at their validity and the regimes where they are applicable.

3.1. Classical correspondence

The simplest way to approach this model is by using classical mechanics and modelling the scatterer as undergoing an impulsive collision with the harmonic oscillator. The impulsive collision is useful to avoid dealing with the restoring force on the harmonic oscillator during the collision itself. The resulting elastic collision conservation equations are

$$p_{x_i} = p_{x_f} + p_y, \tag{6}$$

$$\frac{p_{x_i}^2}{2m} = \frac{p_{x_f}^2}{2m} + \frac{p_y^2}{2M}. \tag{7}$$

p_{x_f} can be eliminated from these equations to obtain

$$p_y = \frac{2p_{x_i}}{1 + \frac{m}{M}}. \tag{8}$$

As an attempt to develop a quantum mechanical approximation for this problem, we can take inspiration from the equations of motions of the coherent state of a quantum harmonic oscillator. Recall that if the time-independent Schrödinger equation [13] is

$$\hat{H}\psi = \frac{p^2}{2M}\psi + \frac{1}{2}M\omega^2 q^2\psi = \omega\left(\hat{a}^\dagger\hat{a} + \frac{1}{2}\right)\psi = E\psi, \tag{9}$$

the annihilation operator is defined as $\hat{a} = \frac{m\omega}{\sqrt{2}}\left(q + \frac{i}{m\omega}p\right)$ and acts on the energy eigenstates of the Hamiltonian as $\hat{a}|n\rangle = \sqrt{n}\,|n-1\rangle$ for integer n. The coherent state is simply an eigenstate of the annihilation operator

$$\hat{a}|\alpha\rangle = \alpha|\alpha\rangle. \tag{10}$$

Coherent states have many ideal properties [14], such as minimum Heisenberg uncertainty $\left(\sigma_p\sigma_q = \frac{\pi}{2}\right)$, and the fact that the expectation of the position and momentum operators follow the classical equations of motion. We can apply the correspondence principle (originally deduced by Schrödinger [15]) to interpret the momentum left behind in the classical harmonic oscillator [15] as the starting momentum of a quantum coherent state. We make this analogy since coherent state evolves in time as

$$\begin{aligned}\alpha(t) &= e^{-i\omega t}\alpha_0 \\ &= |\alpha_0|\cos(\omega t + \measuredangle\phi) - i|\alpha_0|\sin(\omega t + \measuredangle\phi),\end{aligned} \tag{11}$$

where $\alpha_0 = |\alpha_0|\, e^{-i\phi}$. This corresponds to the expectation values of the position and momentum of the coherent state

$$\alpha_C(t) = \sqrt{\frac{M\omega}{2}}\,\langle x(t)\rangle + i\sqrt{\frac{1}{2M\omega}}\,\langle p(t)\rangle. \tag{12}$$

Using the fact that the coherent state is initially at its origin, we deduce the excitation of the quantum harmonic oscillator immediately after collision by setting $\alpha_0 = i\sqrt{\frac{1}{2M\omega}}p_y$. The quantum number population for a coherent state goes as

$$\langle n|\alpha_C\rangle = e^{-|\alpha_C|^2/2}\frac{\alpha_C^n}{\sqrt{n!}} \tag{13}$$

which gives the harmonic oscillator's ground state overlap (using equation (8))

$$|c_0| = |\langle 0|\alpha_C\rangle| = \exp\left(-\frac{1}{M\omega}\frac{p_{x_i}^2}{\left(1 + \frac{m}{M}\right)^2}\right) = \exp\left(-\frac{E_{y_f}}{2\omega}\right), \tag{14}$$

where E_{y_f} is the energy of the harmonic oscillator after collision. This is precisely the probability that the oscillator has left the particle unmeasured, and is the $|c_0|$ given in (5). We can also rewrite this in terms of the initial scatterer energy and the quanta of energy of the harmonic oscillator as

$$|c_0| = \exp\left(-2\frac{m}{M}\frac{E_{\text{scat}}}{\omega\left(1+\frac{m}{M}\right)^2}\right). \tag{15}$$

In the limit of small (m/M) and E_{scat}/ω, this becomes

$$|c_0| \approx 1 - 2\frac{m}{M}\frac{E_{\text{scat}}}{\omega} \tag{16}$$

which indicates that the probability of the scatterer being measured is related to the mass ratio of the scatterer and target and the ratio of energies between the scatterer and the fundamental frequency of the oscillator target.

3.2. Wavefunction reflection

We can make an initial attempt at a quantum mechanical solution by considering the boundary conditions of the problem. The incoming (system+bath) wavefunction in an initially separable state (i.e. with independent coordinates and no coupling)

$$\psi_{\text{in}}(x, y) = \varphi(x)\phi_0(y) = \frac{e^{ik_0 x}}{\sqrt{2\pi}}\phi_0(y) \propto \exp\left(ik_0 x - \frac{1}{2}m\omega y^2\right), \tag{17}$$

where $\phi_0(y)$ is the harmonic oscillator ground state. The true solution will consist of incoming and outgoing wavefunction parts, so to start we perform a coordinate rotation such that, in our new coordinates, the step function becomes

$$\theta\left(x - \sqrt{\frac{m}{M}}y\right) \to \theta\left(\sqrt{1+\frac{m}{M}}x'\right), \tag{18}$$

where the scaled variable in the argument of the step function can be taken out and absorbed into λ. The inverse rotation can be written as

$$\underline{\underline{R}}^{-1}\vec{x_p} = \begin{pmatrix}\alpha & \beta\\ -\beta & \alpha\end{pmatrix}\begin{pmatrix}x'\\ y'\end{pmatrix} = \begin{pmatrix}\alpha x' + \beta y'\\ -\beta x' + \alpha y'\end{pmatrix} = \begin{pmatrix}x\\ y\end{pmatrix}, \tag{19}$$

where $\alpha = \sqrt{\frac{M}{m+M}}$ and $\beta = \sqrt{\frac{m}{m+M}}$. Due to the symmetry of the (rescaled) p_x and p_y and the fact we have performed a unitary transformation, our transformed wavefunction becomes

$$\psi_{\text{in}} \propto \exp\left(ik_0(\alpha x' + \beta y') - \frac{1}{2}m\omega(-\beta x' + \alpha y')^2\right) \tag{20}$$

which remains an eigenstate of the Hamiltonian (2) after the appropriate coordinate transformation has been made to it.

We write the total wavefunction as incoming and outgoing components $\Psi = \psi_{\text{in}} + \psi_{\text{out}}$, and seek to enforce the boundary condition of the problem

$$\begin{aligned}\Psi(x' = 0) = 0 \to \psi_{\text{in}}(x' = 0) &= -\psi_{\text{out}}(x' = 0)\\ &= \exp\left(ik_0\beta y' - \frac{1}{2}m\omega(\alpha y')^2\right).\end{aligned} \tag{21}$$

We now construct an outgoing wavefunction whose plane-wave component travels in the $-\hat{x}$ direction, as though it had been exactly reflected off the hard wall barrier. We write down the trial wavefunction

$$\psi_{\text{out}}(x, y) \propto -\exp\left(-ik_0\beta(\alpha x' - \beta y') - \frac{1}{2}m\omega(-\beta x' + \alpha y')^2\right). \tag{22}$$

The reflection in $\hat{x}$ of the plane-wave part but not the harmonic oscillator part ensures that the harmonic oscillator part of the wavefunction remains properly bounded within the harmonic oscillator potential. We then rotate back to our original coordinates, substitute in $\alpha^2 + \beta^2 = 1$, and plug in the masses for α, β; this yields

$$\psi_{\text{out}}(x, y) \propto -\exp\left(-ik_0\left(\frac{M - m}{M + m}x - \frac{2\sqrt{mM}}{M + m}y\right) - \frac{m\omega}{2}y^2\right) \tag{23}$$

which is shown in figure 3.

We look at the probability amplitude in the free-particle coordinate after averaging over the y-coordinate. In the language of decoherence, this process is known as tracing over the bath to obtain the reduced density matrix (note that we are interested in the diagonal component of the reduced density matrix):

$$\begin{aligned}\rho_{\text{red}}(x, x) &= \int \Psi(x, y)\Psi^*(x, y)dy \\ &= \int (\psi_{\text{in}}(x, y) + \psi_{\text{out}}(x, y))(\psi^*_{\text{in}}(x, y) + \psi^*_{\text{out}}(x, y))dy \\ &= \frac{1}{\pi}\left(1 + e^{-\frac{k_0^2 M}{(m+M)^2\omega}}\cos\left(k_0\frac{2M}{M + m}x\right)\right).\end{aligned} \tag{24}$$

We see a reduction in fringe contrast, implying that the harmonic oscillator 'measured' the incoming scattering particle. This is analogous to placing a weak light source behind the slits of the double slit experiment, as mentioned by Feynman [16]. A recent paper by Kincaid *et al* [17] lucidly described a wavefunction model for a particle travelling through two slits and being measured to a varying degree after emerging from the slits. In both the double slit experiment as with this model, there is a finite chance of measuring the particle which leads to the interference fringes, the wave-like hallmark of quantum systems, becoming quenched, as Kincaid and coauthors described.

We can obtain the result in equation (24) by similar means, using the fact that the harmonic oscillator eigenstates are orthogonal and the harmonic oscillator is in the ground state before the scattering happens. We note the cross term of the integrand in equation (24):

$$\frac{1}{2\pi}e^{-ik_0 x}\int \psi_{\text{out}}(x, y)\phi_0^*(y)dy = \frac{1}{2\pi}e^{-ik_0 x}\widetilde{\psi}_{\text{out}}(x), \tag{25}$$

where we have written a quasi-wavefunction $\widetilde{\psi}_{\text{out}}(x)$. Integrating over the absolute magnitude squared of $\widetilde{\psi}_{\text{out}}(x)$ gives the 'amount' (or rather, the probability) of the wavefunction that remained in the ground state after the scattering:

$$|c_0|^2 = \int |\widetilde{\psi}_{\text{out}}(x)|^2\, dx \tag{26}$$

which yields a more general form

$$|\widetilde{\Psi}(x)|^2 = \frac{1}{\pi}(1 + |c_0|\cos[(k_{\text{in}} + k_{\text{out}})x]). \tag{27}$$

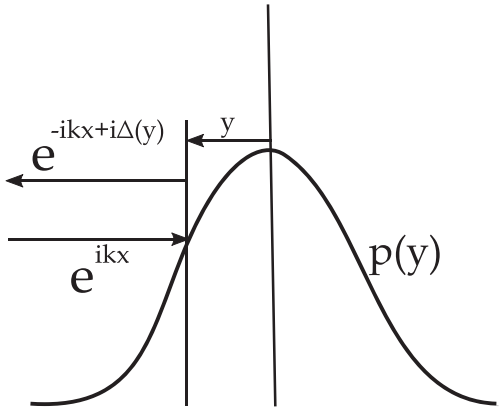

Figure 2. Phase jitter picture—an incoming wave gets reflected at a given y (which introduces phase $\Delta(y)$ to ensure the wavefunction is 0 at the point of collision, with probability $p(y)$.

Rewriting the fringe contrast term in equation (24) gives the ground state overlap as

$$|c_0| = \exp\left(-2\frac{m}{M}\frac{E_{\text{scat}}}{\omega\left(1+\frac{m}{M}\right)^2}\right). \tag{28}$$

It is crucial to note that while the wavefunction given in equation (23) can be an instantaneous solution to the Schrödinger equation, the outgoing wavefunction is not an eigenstate and will not maintain its form under time evolution. Moreover, the trial outgoing wavefunction does not even conserve energy. Nevertheless, this simple attempt at a method-of-images style solution gives not only the classical correspondence but also a gives a quick approximation of the solution.

We finally note that the wavefunction produced by this reflection method is identically a coherent state with the same α as produced with the direct classical mechanical method. To see this, apply the annihilation operator $\hat{a} = \sqrt{\frac{m\omega}{2}}\left(\hat{y} + \frac{i}{m\omega}\hat{p}_y\right)$ to equation (23):

$$\hat{a}\ \psi_{\text{out}} = \frac{ik_0 2\sqrt{M}}{\sqrt{2\omega}\,(M+m)}\psi_{\text{out}} = \alpha_M \psi_{\text{out}}, \tag{29}$$

where we see $|\alpha_C| = |\alpha_M|$ (from (12)).

3.3. Phase jitter approximation

We now model this system using an approach based on the dephasing concepts described by Stern *et al* [18]. In this scheme, we take an input plane wave e^{ikx} and assume that there is a probability $p(y) = |\phi_0(y)|^2$ that the scatterer impacts the harmonic oscillator (originally sitting in its ground state) at the point y. From that point, the scattering plane wave reflects elastically with a simple phase shift dependent on the position of scattering as shown in figure 2. As there is no certain position for the impact to happen, we add all of these probabilities coherently to obtain a pseudo-wavefunction:

$$`\psi(x,\,y)' = \frac{1}{2i}\phi_0(y)(e^{ikx} - e^{-ikx+i\Delta(y)}). \tag{30}$$

As we treat the harmonic oscillator as an impenetrably hard wall, we enforce the condition that $\psi(x = \sqrt{\frac{m}{M}}y) = 0$, or a in equation (5) so that the wavefunction vanishes at the collision point under the hard wall interaction term. This allows us to solve for $\Delta(y) = 2\sqrt{\frac{m}{M}}ky$.

We again trace over the bath (integrating over all possible values of y according to their probabilities) in equation (30) over all possible positions of the harmonic oscillator. Far away from the harmonic oscillator, the probability density becomes

$$\begin{aligned}\mathrm{Tr}_y[|\psi\rangle\langle\psi|] \equiv \rho_{\mathrm{red}}(x,\,x) &= \int \psi^*(x,\,y)\psi(x,\,y)dy \\ &= \frac{1}{4}\left(2 - 2\int \phi_0^*(y)\phi_0(y)\cos(2k(x-y))\right)dy \\ &= \frac{1}{2} - \frac{1}{2}\exp\left(-2\frac{m}{M}\frac{E_{\mathrm{scat}}}{\omega}\right)\cos(2kx),\end{aligned} \tag{31}$$

where $p_x = k$.

Despite the absence of explicit inelastic scattering, the above example demonstrates the diminution of interference fringes induced by the measurement of the scatterer by the harmonic oscillator; in effect, it is a one-particle harmonic bath that measures the scatterer. Note that, for the case where $\left(\frac{m}{M}\right)^2 \ll 1$, we have obtained the same result as in the classical scattering case (16), $|c_0| = \exp\left(-2\frac{m}{M}\frac{E_{\mathrm{scat}}}{\omega}\right) \approx 1 - \frac{2m}{M}\frac{E_{\mathrm{scat}}}{\omega}$.

3.4. Scattering matrix formulation

We can also solve this problem directly using a scattering matrix formalism that explicitly enforces the boundary condition $\psi\left(x = \sqrt{\frac{m}{M}}y\right) = 0$. This wavefunction becomes

$$\psi(x,\,y) = \frac{1}{\sqrt{2}}\left(e^{ik_0x}\phi_0(y) + \sum_n S_{0n}e^{-ik_nx}\phi_n(y)\right), \tag{32}$$

where we have used S_{0n}, borrowing from the conventional S-matrix formalism (S_{0n} refers to the first column of the scattering matrix, whose magnitude squared refers to the probability for the system in state 0 to transition to state n), and k_n is found from the energy conservation condition

$$\frac{k_0^2}{2m} + \frac{1}{2}\omega = \frac{k_n^2}{2m} + \left(n + \frac{1}{2}\right)\omega. \tag{33}$$

Note again that 'incoming' part of the wavefunction is separable (i.e. the two state spaces are completely independent) in the scatterer and the bath, and the 'outgoing' wavefunction consists of the scatterer and the bath entangled together leading to a non-separable state; as Lerner notes, this is a key feature of decoherence [19]. Note also that for an external measurement, the system as prepared exists in all of these states simultaneously until actually measured (see Villars [20]). We enforce the boundary condition $\psi\left(x = \sqrt{\frac{m}{M}}y\right) = 0$ to require

$$e^{ik_0\sqrt{\frac{m}{M}}y}\phi_0(y) + \sum_n S_{0n}e^{-ik_n\sqrt{\frac{m}{M}}y}\phi_n(y) = 0. \tag{34}$$

Note that for purely imaginary $k_u = i\kappa_u$ (the case where $k_0^2/(2m) < u\omega$), the equation still behaves as desired; for $x \to -\infty$ these terms vanish. After solving this equation, we enforce normalisation by ensuring that

$$\sum_{n=0}^{u-1} |S_{0n}|^2 = 1 \tag{35}$$

as the $n \geqslant u$ scattering matrix terms result in vanishingly small contributions due to their finite extent in position space.

We can expand the exponential in the above expression to first order in y as a first approximation. The prefactor on the terms involving y implies that this is equivalent to describing a low energy particle scattering from a heavy particle. After switching notation from $\phi_n(y) \rightarrow \langle y|n\rangle \rightarrow |n\rangle$, we obtain

$$\left(1 + ik_0\sqrt{\frac{m}{M}}y\right)|0\rangle + \sum_n S_{0n}\left(1 - ik_n\sqrt{\frac{m}{M}}y\right)|n\rangle \approx 0. \tag{36}$$

Using the harmonic oscillator relations $y = \sqrt{\frac{1}{2m\omega}}(\hat{a} + \hat{a}^\dagger)$, where $\hat{a}$ and $\hat{a^\dagger}$ are again the raising and lowering operations of the harmonic oscillator, and defining (for clarity of notation) $g = \sqrt{\frac{m}{M}}$ and applying these operators to the above expression yields the system of equations

$$(|0\rangle + ik_0 g|1\rangle) + \sum_n S_{0n}(|n\rangle - ik_n g\sqrt{n+1}\,|n+1\rangle - ik_n g\sqrt{n}\,|n-1\rangle) = 0. \tag{37}$$

If we take the inner product with each state $\langle n'|$, we can obtain the following system of equations for $\langle 0|$, $\langle 1|$, and $\langle n|$ with $n > 1$:

$$\begin{aligned} 1 + S_{00} - ik_1 g S_{01} &= 0 \\ ik_0 g + S_{01} - ik_0 g S_{00} - ik_2 g\sqrt{2}\,S_{02} &= 0 \\ S_{0n} - ik_{n-1} g\sqrt{n}\,S_{0,n-1} - ik_{n+1} g\sqrt{n+1}\,S_{0,n+1} &= 0. \end{aligned} \tag{38}$$

To solve this system of linear equations we can truncate the series to n' terms by setting $S_{0,n'} = 0$ (making sure that our solution has converged).

For the lowest order solution, we truncate our series with $S_{02} = 0$. This refers to the case where the scatterer is a low energy particle that does not deposit more than one quanta of energy to the stiff, high frequency oscillator of large mass. In this case, we obtain

$$S_{00} = -\frac{1 - (k_0 k_1)/(2M\omega)}{1 + (k_0 k_1)/(2M\omega)}. \tag{39}$$

We can obtain the fringe contrast by looking at the quantity $|S_{00}|^2$. For the case where $k_0^2/2m > \omega$ we obtain

$$|S_{00}| = 1 - 2\frac{E_{\text{scat}}}{\omega}\frac{m}{M}, \tag{40}$$

where we regain the result from classical scattering (15) in the limit where $\sqrt{m/M} \ll 1$ and $E_{\text{scat}}/\omega \ll 1$. In the case where $E_{\text{scat}} < \omega$, we swap $k_1 \rightarrow \kappa_1$ and equation (40) becomes

$$S_{00} = -\frac{1 - i(k_0\kappa_1)/(2M\omega)}{1 + i(k_0\kappa_1)/(2M\omega)} \tag{41}$$

so that $|S_{00}| = 1$. This is fundamentally different from the classical case, as the incoming plane wave does not have enough energy to excite the harmonic oscillator mode and the scattering process results solely in a phase shift.

We can also derive an exact solution for the scattering matrix solution. Instead of expanding equation (34) to first order in $k_0\sqrt{\frac{m}{M}}y$, we simply take the inner product to instead obtain

$$\langle m|e^{ik_0\sqrt{\frac{m}{M}}y}|0\rangle + \sum_n S_{0n}\langle m|e^{-ik_n\sqrt{\frac{m}{M}}y}|n\rangle = 0. \tag{42}$$

We have from before that $y = \sqrt{\frac{1}{2m\omega}}(\hat{a} + \hat{a}^\dagger)$. We can use the Baker–Campbell–Hausdorff formula [21], noting the quantum harmonic oscillator commutator relation $[\hat{a}, \hat{a}^\dagger] = 1$ and the fact higher order commutators hence vanish, to rewrite $e^{ik_0\sqrt{\frac{m}{M}}y}$ as

$$\begin{aligned} e^{ik_0\sqrt{\frac{m}{M}}y} &= e^{ik_0\sqrt{\frac{1}{2M\omega}}(\hat{a}^\dagger+\hat{a})} \\ &= e^{-\frac{k_0^2}{4M\omega}}e^{ik_0\sqrt{\frac{1}{2M\omega}}\hat{a}^\dagger}e^{ik_0\sqrt{\frac{1}{2M\omega}}\hat{a}} \end{aligned} \tag{43}$$

and similarly for $e^{-ik_n\sqrt{\frac{m}{M}}y}$. This yields the inner product

$$\langle m|e^{ik_0\sqrt{\frac{m}{M}}y}|n\rangle = e^{-\frac{k_0^2}{4M\omega}}\langle m|e^{ik_0ga^\dagger}e^{ik_0ga}|n\rangle. \tag{44}$$

We can apply the right-hand operator to the ket and the left hand operator on the bra separately. The ket part of the expression becomes

$$e^{ik_0\sqrt{\frac{1}{2M\omega}}a}|n\rangle = \sum_{\ell=0}^{n}\frac{1}{\ell!}\sqrt{\frac{n!}{(n-\ell)!}}(ik_0g)^\ell|n-\ell\rangle \tag{45}$$

and the bra part of the expression becomes (noting the required complex conjugation):

$$e^{-ik_0\sqrt{\frac{1}{2M\omega}}a}|m\rangle = \sum_{p=0}^{m}\frac{1}{p!}\sqrt{\frac{m!}{(m-p)!}}(-ik_0g)^p|m-p\rangle. \tag{46}$$

We can use the orthogonality of states $\langle m-p|n-\ell\rangle = \delta_{n-\ell,m-p}$ to obtain the inner product:

$$\langle m|e^{ik_0\sqrt{\frac{m}{M}}y}|n\rangle = \begin{cases} e^{-\frac{k_0^2}{4M\omega}}\sum_{\ell=0}^{n}\frac{\sqrt{n!\,m!}(ik_0g)^{m-n+2\ell}}{(n-\ell)!\,\ell!\,(m-n+\ell)!} & \text{if } m \geqslant n \\ e^{-\frac{k_0^2}{4M\omega}}\sum_{\ell=0}^{m}\frac{\sqrt{n!\,m!}(ik_0g)^{n-m+2\ell}}{(m-\ell)!\,\ell!\,(n-m+\ell)!} & \text{otherwise} \end{cases} \tag{47}$$

which we can plug into equation (42) to solve for the exact solution to the scattering matrix.

Once we solve for the scattering matrix components S_{0n}, we can evaluate the wavefunction

$$\psi(x, y) = \frac{1}{\sqrt{2}}\left(e^{ik_0x}\phi_0(y) + \sum_n S_{0n}e^{-ik_nx}\phi_n(y)\right). \tag{48}$$

If we express this sum in terms of the kets, this becomes

$$|\psi\rangle = \frac{1}{\sqrt{2}}\left(|k_0\rangle|0\rangle + \sum_n S_{0n}|-k_n\rangle|n\rangle\right) \tag{49}$$

which yields the density matrix

$$\begin{aligned} \rho = |\psi\rangle\langle\psi| = \frac{1}{2}\Bigg(&|k_0\rangle|0\rangle\langle 0|\langle k_0| + \sum_n S_{0n}|-k_n\rangle|n\rangle\langle 0|\langle k_0| \\ &+ \sum_n S_{0n}^*|k_0\rangle|0\rangle\langle n|\langle -k_n| + \sum_{nm} S_{0m}^*S_{0n}|k_n\rangle|n\rangle\langle m|\langle -k_m|\Bigg). \end{aligned} \tag{50}$$

If we trace out the bath coordinate (or, sum over the diagonal entries of the bath states), we obtain the reduced density matrix

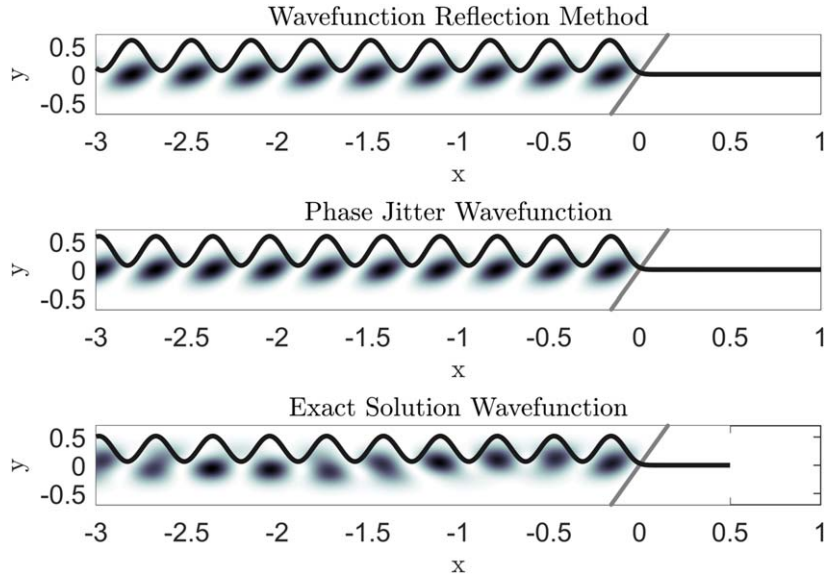

Figure 3. Analytical wavefunction and density matrix comparison—we compare the wavefunction magnitude in the x–y plane as well as the reduced density after tracing over the bath $\int |\psi(x, y)|^2 dy$ for each of the analytical techniques described.

$$\rho_{\text{red}} = \text{Tr}_{\text{bath}}[|\psi\rangle\langle\psi|] = \frac{1}{2}\left(\left| 0\rangle\langle 0| + S_{00}|k_0\rangle\langle -k_0| + S_{00}^* \right| - k_0\rangle\langle k_0| + \sum_n |S_{0n}|^2 \right| - k_n\rangle\langle k_n \left| \right| \right). \quad (51)$$

We can see that in the case where $|S_{00}| < 1$, the wavevectors corresponding to excitations of the oscillator have no off-diagonal coupling to the original wavevector, the tell-tale sign of decoherence.

3.5. Technique comparison

We can compare the wavefunctions produced by these techniques, shown for $m = 1$, $M = 20$, $\omega = 20$, $E = 50$ (a case with a relatively heavy target with a moderately stiff spring) in figure 3, with the diagonal part of the reduced density matrix (the probability for the system coordinates averaged over the bath coordinates) plotted on top.

The first two wavefunctions plotted in figure 3 are those produced by the intuitive physical arguments presented (wavefunction reflection and phase jitter). The wavefunctions are tilted in the y-direction from the ground state harmonic oscillator which yields a reduction in fringe contrast after averaging over y. The wavefunctions are similar, with the phase jitter model producing a smaller wavelength as mentioned before. Despite their pleasing visage, these wavefunctions are not energy eigenstates. The last wavefunction, the exact solution, has a radically different character that still yields a comparable fringe contrast. Close to the barrier, it has strong resemblance to the previous heuristic wavefunctions, but the similarity ends there as the tilt in y oscillates in x space.

We then examine the fringe contrast versus energy, in figure 4.

The first thing to note is that for low energies the classical and phase jitter pictures are very similar with a slightly different slope due to the additional factor of $\left(1 + \frac{m}{M}\right) \approx 1.10$ in the exponent of equation (15). However, for $E < 20$, the quantum mechanical results (both

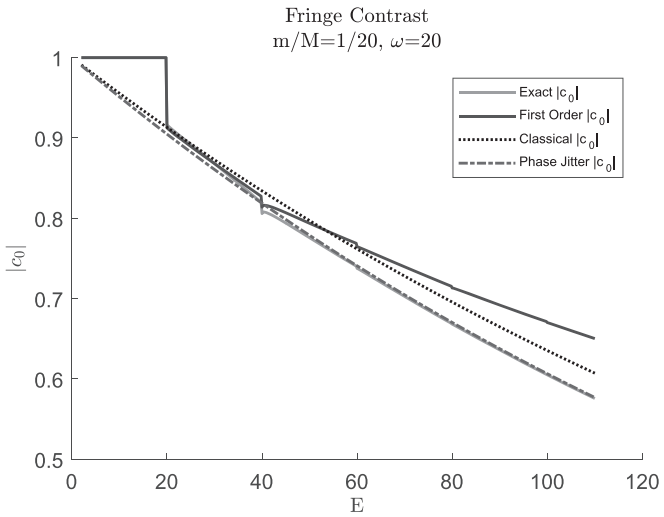

Figure 4. Fringe contrast versus energy—$|c_0|$ is both the square root of the probability of the target remaining in the ground state as well as being a direct indicator of the remaining wave-like character of the wavefunction.

the exact and the first order results) have no diminution in fringe contrast. This is a demonstration of one of the fundamental aspects of quantum mechanics: for energies less than the fundamental frequency there is no possibility of exciting the scattering target and the only far-field effect of scattering is a phase shift. This is analogous to Einstein's photoelectric effect (and indeed, light fields are treated as harmonic oscillators in quantum electrodynamics).

For energies above the fundamental ($E > \omega$), the exact and first order quantum results abruptly drop off in the fringe contrast to match those of the fringe contrast predicted by the classical value. As the energy increases, the exact and first order results initially match those of the strictly classical result (as discussed above). As the energy increases to the second harmonic of the oscillator, there is a small transient dip at $E = 40$ indicating a resonance at that energy. Above this energy the behaviour has shifted; the exact result tracks the fringe contrast predicted by the phase jitter picture quite well, which confirms our intuition that this model is valuable for larger energy, higher excitation situations. Furthermore, it is clear that the first order model has broken down by this point; it begins to diverge from the exact result and overestimates the fringe contrast remaining in the system dynamics. This is to be expected however, as our expansion condition for equation (36) is $k_0\sqrt{\frac{m}{M}}y \approx \frac{m}{M}\sqrt{\frac{4E}{\omega}} \ll 1$. At $E \approx 40$ this constant is approximately 0.14, which is roughly where we would expect this model to diverge from the exact solution.

4. Numerical approaches

The enormous power of modern computers has opened up huge possibilities for simulating physical systems. We introduce here several methods for solving a modified version of the simple decoherence model presented here. We first demonstrate the split-operator approximation for evolving quantum mechanics and show how to use the fast Fourier transform to solve it in multiple dimensions. We then show the exact solution for the harmonic oscillator

with a time-dependent forcing function. We next introduce the thawed Gaussian approximation [22], the solution of a Gaussian wavepacket in a potential that we treat as periodic at all times. We then discuss the modifications to our model to accommodate the methods we are using and present the results of the numerical simulations.

4.1. Split-operator FFT

One of the most straightforward methods to numerically solve the Schrödinger equation in low dimensionality is the split-operator fast Fourier transform (SOFFT) method. The scheme for performing the unitary evolution of the wavefunction in two-dimensions can be expressed as

$$\langle xy|\psi(t+\Delta t)\rangle \approx \langle xy|e^{-i\hat{H}\Delta t}|\psi(t)\rangle, \tag{52}$$

where the approximately equal sign becomes exactly equal when the Hamiltonian commutes with itself for all time [21]. We assume that our Hamiltonian is separable in position and momentum:

$$\hat{H}(\hat{p},\hat{q}) = \hat{T}(\hat{p}) + \hat{V}(\hat{x}). \tag{53}$$

For the case where where $[\hat{T},\hat{V}] \ll \Delta t^{-2}$, we may approximately (see [23]) write equation (52) as

$$e^{-i\hat{H}\Delta t} \approx e^{-i\hat{T}(\hat{p})\Delta t/2}e^{-i\hat{V}(\hat{x})\Delta t}e^{-i\hat{T}(\hat{p})\Delta t/2}. \tag{54}$$

It is known from linear algebra that a vector represented in an orthogonal basis can be represented by any other orthogonal basis of the vector space [21]. We rewrite equation (52) using approximation (54) by inserting complete sets of operator states (defining $\vec{x} = (x, y)$ and $\vec{p} = (p_x, p_y)$)

$$\begin{aligned}\langle\vec{x}|\psi(t+\Delta t)\rangle = \int \langle\vec{x}|\vec{p}\,\rangle\langle\vec{p}\,|e^{-i\hat{T}\Delta t/2}|\vec{p}\,'\rangle\langle\vec{p}\,'|\vec{x}\,'\rangle \\ \langle\vec{x}\,'|e^{-i\hat{V}\Delta t}|\vec{x}\,''\rangle\langle\vec{x}\,''|\vec{p}\,''\rangle\langle\vec{p}\,''|e^{-i\hat{T}\Delta t/2}|\vec{p}\,'''\rangle \\ \langle\vec{p}\,'''|\vec{x}\,'''\rangle\langle\vec{x}\,'''|\Psi(t)\rangle\, d\vec{x}\,'''d\vec{p}\,''' \ldots\end{aligned} \tag{55}$$

With our assumption that the kinetic energy operator $\hat{T}$ depends on the momenta and the potential operator $\hat{V}$ depends solely on position, the matrix elements $\langle p_x p_y|e^{-i\hat{T}\Delta t/2}|p_x' p_y'\rangle$, etc become diagonal in their respective bases. We have effectively reduced the problem from the multiplication of a matrix by a vector to that of multiplying a vector by a vector. The only remaining challenge is performing the repeated Fourier transforms, as expressed by the terms $\langle p_x p_y|xy\rangle = \frac{1}{2\pi}e^{-ip_x x - ip_y y}$. Evolving the wavefunction by performing the above integral yields the following algorithm:

1. Fourier transform the initial wavefunction $\mathcal{F}\{\psi_a\} \rightarrow \widetilde{\psi_a}$.
2. Apply $e^{-i\hat{T}\Delta t/2}$ to $\widetilde{\psi_a} \rightarrow \widetilde{\psi_b}$
3. Perform the inverse Fourier transform $\mathcal{F}^{-1}\{\widetilde{\psi_b}\} \rightarrow \psi_b$
4. Apply $e^{-i\hat{V}\Delta t}$ to $\psi_b \rightarrow \psi_c$
5. Fourier transform $\mathcal{F}\{\psi_c\} \rightarrow \widetilde{\psi_c}$.
6. Apply $e^{-i\hat{T}\Delta t/2}$ to $\widetilde{\psi_c} \rightarrow \widetilde{\psi_d}$
7. Perform the inverse Fourier transform $\mathcal{F}^{-1}\{\widetilde{\psi_d}\} \rightarrow \psi_d$

The principal advantage of this scheme is computational time. For a generic Hamiltonian in D dimensions and represented by N points per dimension, the storage requirement for the

Hamiltonian is $\mathcal{O}(N^{2\mathrm{D}})$ and the evolution of the wavefunction is $\mathcal{O}(N^{2\mathrm{D}})$ per time step. However, using this scheme we may reduce the storage requirement to $\mathcal{O}(N^{\mathrm{D}})$ and reduce the computational time per step from $\mathcal{O}(N^{2\mathrm{D}})$ to $\mathcal{O}((N\log N)^{\mathrm{D}})$. This is one valuable application of the fast Fourier transform, which has been described [24] as 'the most important numerical algorithm of our lifetime.' Higgins [25] describes many interesting facets of the FFT algorithm, from describing the periodicity of the exponential inherent to the algorithmic speedup as well as pitfalls that can emerge from the naive use of a discrete Fourier transform (such as the spectral width of sinusoids at integer and noninteger multiples of the fundamental frequencies).

The continuous Fourier transform of the wavefunction is

$$\widetilde{\psi}(p_x, p_y) = \frac{1}{2\pi}\int e^{-ip_x x}e^{-ip_y y}\psi(x, y)dx\, dy. \tag{56}$$

We are interested in performing this transformation along a finite grid. After evenly discretizing the lattice as N_x and N_y discrete points x_α and y_β, our expression becomes

$$\langle p_{x_\mu} p_{y_\nu}|\psi\rangle = \frac{\Delta x\Delta y}{2\pi}\sum_{\alpha\beta} e^{-ip_{x_\mu}x_\alpha}e^{-ip_{y_\nu}y_\beta}\langle x_\alpha y_\beta|\psi\rangle. \tag{57}$$

We can write the discretization as

$$\begin{aligned} x_\alpha &= x_{\min} + \alpha\Delta x \\ p_{x_\mu} &= p_{x_{\min}} + \mu\Delta p_x \\ y_\beta &= y_{\min} + \beta\Delta y \\ p_{y_\nu} &= p_{y_{\min}} + \nu\Delta p_y. \end{aligned} \tag{58}$$

Writing the wavefunction ψ as a matrix in row-column form as $\psi_{\beta\alpha}$ where row β refers to the y index and column α refers to the x index and rearranging terms in the exponential, we obtain

$$\begin{aligned} \widetilde{\psi_{\nu\mu}} = {} & \frac{\Delta x\Delta y}{2\pi}e^{-ip_x x_{\min} - ip_y y_{\min} - i\mu\Delta p_x x_{\min} - i\nu\Delta p_y y_{\min}} \\ & \sum_{\alpha\beta} e^{-i\mu\alpha\Delta p_x\Delta x - i\nu\beta\Delta p_y\Delta y}(e^{-ip_{x_{\min}}\alpha\Delta x - ip_{y_{\min}}\beta\Delta y}\psi_{\beta\alpha}). \end{aligned} \tag{59}$$

The general form of the FFT command `y=fft(x)` in typical numerical programs [26] is

$$y_k = \sum_{j=0}^{n-1} x_j e^{-i(2\pi jk/n)}. \tag{60}$$

So, we apply the FFT algorithm to the expression in parentheses in equation (59), first transforming the rows and then the columns. This sets restrictions for the relationship between Δx and Δp_x, forcing $\Delta p_x\Delta x = 2\pi/N_x$, and hence enforcing the range of the momentum for our simulations to be $p_{x_{\max}} - p_{x_{\min}} = (N_x - 1)\Delta p_x$

4.2. Forced harmonic oscillator

We may also reuse the analogy from section 3.1 of treating the classical position and momentum as the real and imaginary components of a coherent state in a harmonic well. Instead of an instantaneous collision, we instead evolve the classical equations of motion and use the force between the oscillator and the scatterer to drive the coherent state. This is an important physical system that has been derived in many forms [27–30] and has applications ranging from atomic physics to quantum electrodynamics. We rewrite the Hamiltonian in

terms of only the oscillator coordinate and the effective force on it, as

$$\begin{aligned}\hat{H}_{\text{eff}} &= \frac{p_y^2}{2m} + \frac{1}{2}m\omega^2 y^2 + y f_y(t) \\ &= \omega \hat{a}^\dagger \hat{a} + \frac{f(t)}{\sqrt{2\,m\omega}}(\hat{a} + \hat{a}^\dagger).\end{aligned} \tag{61}$$

We conjecture the solution is a harmonic oscillator coherent state $|z\rangle$ whose eigenvalue is time-dependent:

$$|\tilde{z}(t)\rangle = |z(t)e^{-i\omega t}\rangle = \sum_n \frac{\tilde{z}^n}{\sqrt{n!}} \exp\left(-\frac{1}{2}|z|^2 - ig(t)\right)|n\rangle, \tag{62}$$

where the yet-to-be determined $g(t)$ is the Maslov phase. Writing the Schrödinger equation $\hat{H}|\tilde{z}\rangle = i\frac{\partial}{\partial t}|\tilde{z}\rangle$ yields, after rearrangement

$$\begin{aligned}&\sum_{n=0}^{\infty}\left(n\omega + \frac{\tilde{z}f(t)}{\sqrt{2\,m\omega}}\right)\frac{\tilde{z}^n}{\sqrt{n!}}|n\rangle + \left(\frac{f(t)}{\sqrt{2m\omega}}\frac{\tilde{z}^n}{\sqrt{n!}}\right)|n+1\rangle = \\ &\sum_{n=0}^{\infty}\left(\frac{-i}{2}\left(z^*\frac{\partial z}{\partial t} + z\frac{\partial z^*}{\partial t}\right) + \frac{\partial g}{\partial t} + i\frac{n}{z}\frac{\partial z}{\partial t} + n\omega\right)\frac{\tilde{z}^n}{\sqrt{n!}}|n\rangle.\end{aligned} \tag{63}$$

As the harmonic oscillator eigenstates are orthogonal, we can multiply on the right-hand side by $\langle 0|$, and $\langle n|$ (with $n > 0$). Subtracting the former equation from the latter, we obtain

$$\frac{\partial z}{\partial t} = -i\frac{f(t)e^{i\omega t}}{\sqrt{2\,m\omega}} \tag{64}$$

which can be solved to obtain

$$z(t) = z_0 - \frac{i}{\sqrt{2\,m\omega}}\int_{-\infty}^{t} f(t')e^{i\omega t'}dt'. \tag{65}$$

Plugging this solution for $z(t)$ back into the collected terms for $|0\rangle$ and using $\langle y(t)\rangle = \frac{1}{\sqrt{2m\omega}}(\tilde{z} + \tilde{z}^\dagger)$, we obtain the Maslov phase

$$g(t) = g_0 - \frac{1}{2}\int_{-\infty}^{t}\langle y(t')\rangle f(t')dt'. \tag{66}$$

4.3. Thawed Gaussian approximation

While the split-operator FFT method is a valuable and powerful method for 'exactly' (within numerical precision) evolving position-momentum separable quantum mechanical systems, it suffers from complexity that scales geometrically with dimension (as do all grid-based approach to numerical simulations). The forced harmonic oscillator method, while useful in many contexts, completely disregards the behaviour and effect on the scatterer and neglects all quantum effects. We can introduce different approximations in order to simulate quantum mechanical systems in higher dimensionality. One straightforward method for approximating quantum mechanical dynamics is the thawed Gaussian approximation [22]. The core principle is that the wavefunction is treated at all times as a Gaussian wavepacket given by

$$\Psi(\vec{x}, t) = \exp\left(i(\vec{x} - \vec{x}_t)^\top \underline{\underline{\alpha_t}}(\vec{x} - \vec{x}_t) + i\vec{p}_{x_t}^{\top}(\vec{x} - \vec{x}_t) + i\gamma_t\right) \tag{67}$$

and evolves in a potential that is taken to be quadratic about the central guiding trajectory at all times

$$\hat{H}_{\mathrm{TGA}} = \sum_n \frac{\vec{p}_n^{\,2}}{2m_n} + V(\vec{x}_t) + \frac{\partial V}{\partial \vec{x}}\bigg|_{\vec{x}=\vec{x}_t} (\vec{x} - \vec{x}_t) + \frac{1}{2}(\vec{x} - \vec{x}_t)^{\top} \frac{\partial^2 V}{\partial \vec{x}\partial \vec{x}}\bigg|_{\vec{x}=\vec{x}_t} (\vec{x} - \vec{x}_t). \tag{68}$$

Here $\vec{x}_t$ and $\vec{p}_t$ evolve according to Hamilton's equations [31]

$$\begin{aligned} \dot{x}_t &= \frac{p_t}{m} \\ \dot{p}_t &= -\frac{\partial V}{\partial x}\bigg|_{x=x_t}. \end{aligned} \tag{69}$$

The covariance matrix α_t evolves as

$$\dot{\underline{\underline{\alpha}}}_t = -2\,\underline{\underline{\alpha}}_t \underline{\underline{m}}^{-1} \underline{\underline{\alpha}}_t - \frac{1}{2}\frac{\partial^2 V}{\partial \vec{x}\partial \vec{x}}\bigg|_{\vec{x}=\vec{x}_t}, \tag{70}$$

where $\underline{\underline{m}}$ is a diagonal matrix of each of the particles' masses. The phase γ_t evolves in time to preserve the wavefunction normalisation and include the accumulated action

$$\dot{\gamma}_t = i\,\mathrm{Tr}[\underline{\underline{m}}^{-1} \underline{\underline{\alpha}}_t] + \mathcal{L}_t, \tag{71}$$

where Tr denotes the trace and $\mathcal{L}_t$ is the Lagrangian of the system evaluated at time t. This algorithm has the advantage that the complexity required for simulation becomes $\mathcal{O}(D^3)$, giving power law scaling instead of geometric scaling. This makes this method a very attractive approach for studying many-particle systems [32], as is frequently done in quantum physical chemistry. For further reading, another presentation of the evolution of Gaussian wavepackets is given by Balasubramanian [33] for the case of a particle in an electric field; this is mathematically equivalent to setting $\frac{\partial^2 V}{\partial x^2} = 0$.

4.4. Time-dependent evolution details

Several tweaks must be made to the original problem when using the above time-dependent methods. When we performed the calculations for the analytic case, we made the approximation that the interaction potential was $V(x, y) = \lambda\theta(x - y)$ with $\lambda \to \infty$; or rather, that the potential used at the moment of interaction was a hard wall. This potential could be incorporated into the split-operator method by performing a coordinate rotation and noting that the edges in a straightforward SOFFT computation act as perfectly reflecting barriers. However, this approach would be poor for the thawed Gaussian approximation due to its inability to compensate for the analytical discontinuity in the step function. This restriction can however be physically advantageous as there are no true hard wall potentials, either at the classical level or certainly the microscopic level. We therefore analyse the problem of a free particle coming from $-\infty$ impacting a harmonic oscillator with an exponentially repulsive interaction potential:

$$\hat{H} = \frac{p_x^2}{2m} + \frac{p_y^2}{2M} + \frac{1}{2}M\omega^2 y^2 + A\exp[\beta(x - y)]. \tag{72}$$

The choice of the exponential parameters A and β alter the behaviour of the potential. Larger β will serve to create a sharper, more sudden interaction while a smaller β yields a less impulsive collision, which acts to reduce the harmonic oscillator excitation as we will see in the results. The choice of A determines the exact location of where the scatterer reflection takes place and is less critical.

When we performed the analytical calculations, we were able to describe a single monoenergetic wavevector and analyse its decoherence properties. Clearly for the thawed Gaussian approximation but less obviously so for the split-operator method, this is not directly feasible. This is a consequence of the fact that we have switched to the time evolution picture of quantum mechanics, and a single energy requires infinite time to capture correctly per $\Delta E \Delta\ t \geqslant \hbar/2$. However, we can go to the energy-domain by looking at the Fourier transform of the time-dependent wavefunction:

$$\psi(x,\, y,\, E) = \int_{-\infty}^{\infty} e^{iEt}\psi(x,\, y,\, t)\, dt. \tag{73}$$

In the case of a time-independent Hamiltonian, we can use the time evolution operator to express this as

$$\begin{aligned}\psi(x,\, y,\, E_j) &= \int_{-\infty}^{\infty} e^{iE_j t}e^{-i\hat{H}t}\psi(x,\, y,\, t = -\infty)dt \\ &= \sum_k \int_{-\infty}^{\infty} e^{iE_j t}e^{-iE_k t}c_k\Phi_{E_k}(x,\, y)\, dt \\ &\propto \sum_{E_k = E_j} c_k\Phi_{E_k}(x,\, y),\end{aligned} \tag{74}$$

where the Φ_{E_k} refers to the (possibly degenerate) energy eigenstates of the Hamiltonian with energy E_k. Thus, the time-domain Fourier transform filters out the 'amount' of a particular energy, and the position space energy eigenfunctions contained in an arbitrary wavefunction. For finite evolution with non-infinitesimal time steps, this becomes an approximation:

$$\psi(x,\, y,\, E) \approx \Delta t \sum_n e^{iEt_n}\psi(x,\, y,\, t_n), \tag{75}$$

where the energy range is dictated by the time step used $\left(E_{\max} = \frac{\pi}{\Delta t}\right)$ and the energy resolution is dictated by total time of evolution $\left(\Delta E = \frac{\pi}{N\Delta t}\right)$.

While this transform is a relatively expensive numerical operation, it is straightforward to perform in low dimensionality. Moreover, if one opts to use a larger energy spread for the initial wavepacket, one can transform on multiple energies for the same simulation run. Using the known general behaviour of the wavefunction from equation (32), we may cast this wavefunction (away from the interaction region) as

$$\psi(x,\, y,\, E) \approx e^{ik_0 x}\phi_0(y) + \sum_n c_n e^{-ik_n x}\phi_n(y), \tag{76}$$

where $k_0 = \sqrt{2\, mE}$. From this we can look at the diagonal elements of the reduced density to obtain the wavefunction:

$$\rho_{\text{red}}(x,\, x) = \text{Tr}_y[|\psi\rangle\langle\psi|] = 1 + |c_0|\cos(2k_0 x + \delta), \tag{77}$$

where δ is an arbitrary phase. The fringe contrast is clearly equivalent to $|c_0|$, as in equation (5).

We can now use the tools that we have described in order to obtain numerical results for this problem. We choose a fairly steep potential, with $\beta = 8$ and $A = 2000$, examining the

behaviour versus energy using the energy range 2–120 eV. The choice of β was chosen to ensure that the thawed Gaussian wavefunction retained unit normalisation throughout its evolution; higher incident energies will have smaller interaction times and hence approach the results of the infinite hard wall. The choice of A was chosen to prevent the scatterer wavefunction from entering the region $x > y$ which we treat as unphysical. We used the same initial starting position for each value of energy, and we used the same position space grid of 2048×64 for all energies considered.

It then becomes necessary to choose the initial value of $\underline{\underline{\alpha}}$ in equation (67) for our simulations; we use the same initial wavefunction for both the split operator and thawed Gaussian methods. The first obvious choice is to assume an initially separable (and hence, without correlations between coordinates) state $\phi(x)\varphi(y)$, which dictates $\alpha_{xy} = 0$. For the target harmonic oscillator coordinate, the natural choice was to choose $\alpha_y = iM\omega/2$, which corresponds to the ground state of the harmonic oscillator. For the free scatterer coordinate we chose α_x such that the wavefunction would collect itself to its narrowest point at the turn-around point in order to improve the validity of the thawed Gaussian method; Blinder [34] describes the collection and spreading of a Gaussian in free space directly by using an operator analogous to the momentum-translation. For the thawed Gaussian approximation to be reasonable (the potential being approximately quadratic along the stretch of the potential) it was necessary to use a large value of α_0 so that the wavepacket could be spatially small at the point of impact. The consequence of this, due to the Heisenberg uncertainty principle $\Delta x \Delta p \geqslant \hbar$ (which is in turn a mathematical consequence of Fourier transforms), is a large position spread at the beginning and end of the simulation due to the large momentum spread of the wavefunction. However, we wanted the wavefunction to be initially 0 in the region of the interaction potential; this ensured the concurrent requirement that the momentum of the wavepacket was restricted to $p > 0$. As a compromise, we used the 'target' at collision wavepacket spread to be $\alpha_{xx} = iE/8$ which ensures a momentum spread that was approximately completely positive.

4.5. Technique comparison

We evolved the wavefunctions under these two regimes using these initial conditions. A demonstration of the wavefunction amplitudes versus time is given in figure 5.

Here t_c is the time at closest approach and t_f is the final time evaluation. At the collection time, the thawed Gaussian approximation is rather poor; the wavefunction bleeds into the exponential repulsive region to a far greater degree than is physically reasonable; as compared to the 'exact' split-operator-evolved wavefunction. Nevertheless, despite this moment of non-physical behaviour, the final wavefunctions have very similar character. This is robust across many energies and improves with higher energies. This is demonstrated in figure 6 where we plot the wavefunction overlap $|\langle \Psi_{\mathrm{FFT}} | \Psi_{\mathrm{TGA}} \rangle|$.

As we can see, the overlap between the thawed Gaussian and split-operator time-evolved wavefunctions gets better with increasing energies; with the parameters we chose, the energy spread of the wavefunction increases with incident scatterer energy, thus allowing the wavefunction to collect to a smaller spread at the point of collision. The thawed Gaussian approximation still remains incapable of preventing the wavepacket from occupying the energetically forbidden region. Nonetheless, the final wavefunction in general does a good job capturing the degree of excitation of the harmonic oscillator.

As mentioned, we can go from a time-domain wavefunction to an energy-domain wavefunction by Fourier transforming the wavefunction with respect to time; this allows us to determine 'amount' of a given energy in a given eigenstate. We do this for one run using a

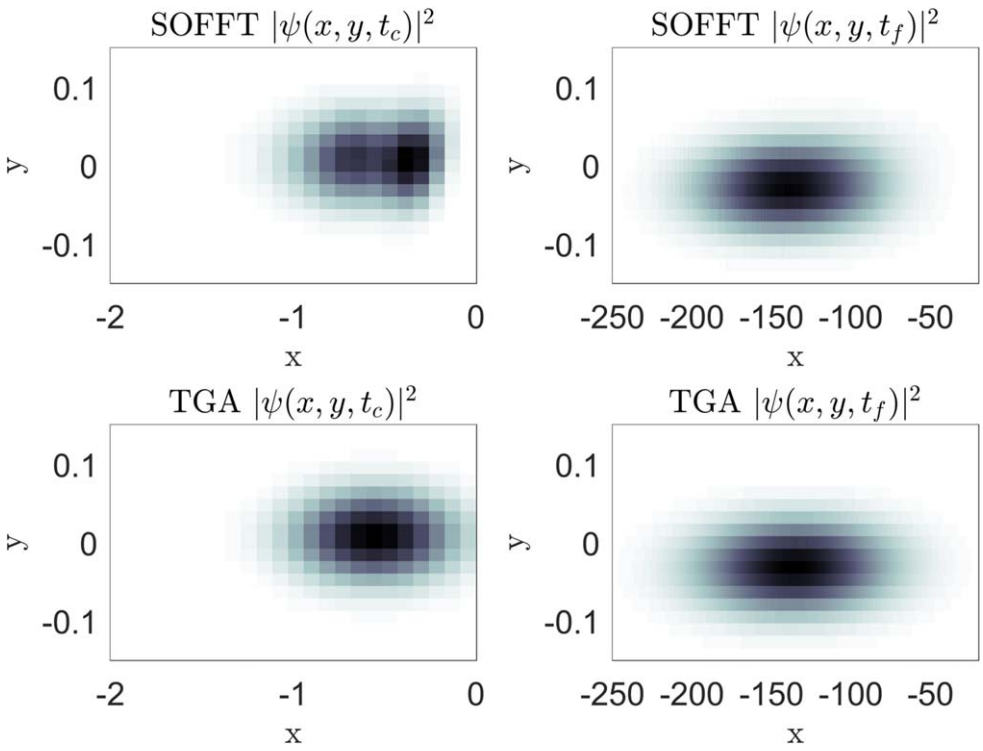

Figure 5. SOFFT versus TGA wavefunction comparison ($E_{\text{scat}} = 50$)—we plot here the absolute magnitude of the split operator and thawed Gaussian wavefunction both at the instant of closest interaction (t_c) as well as at the end of the simulation (t_f). Note the unphysical spreading of the thawed Gaussian beyond the exponential wall.

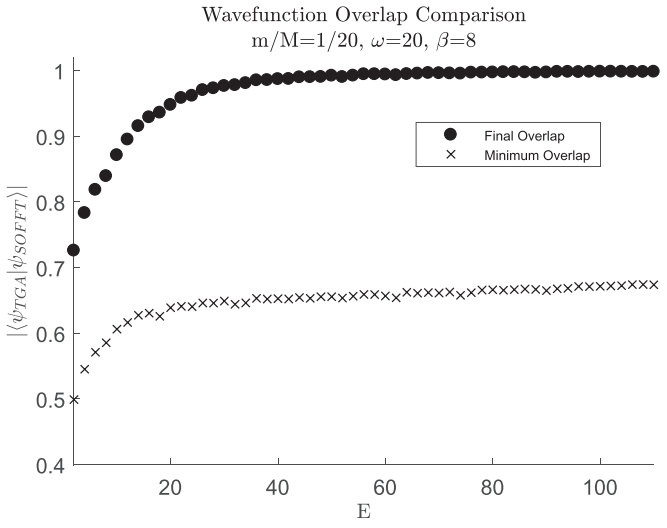

Figure 6. Overlap comparison $|\langle\psi_{\text{TGA}}|\psi_{\text{SOFFT}}\rangle|$ versus scatterer central energy at both the instant of closest interaction and after the interaction is finished.

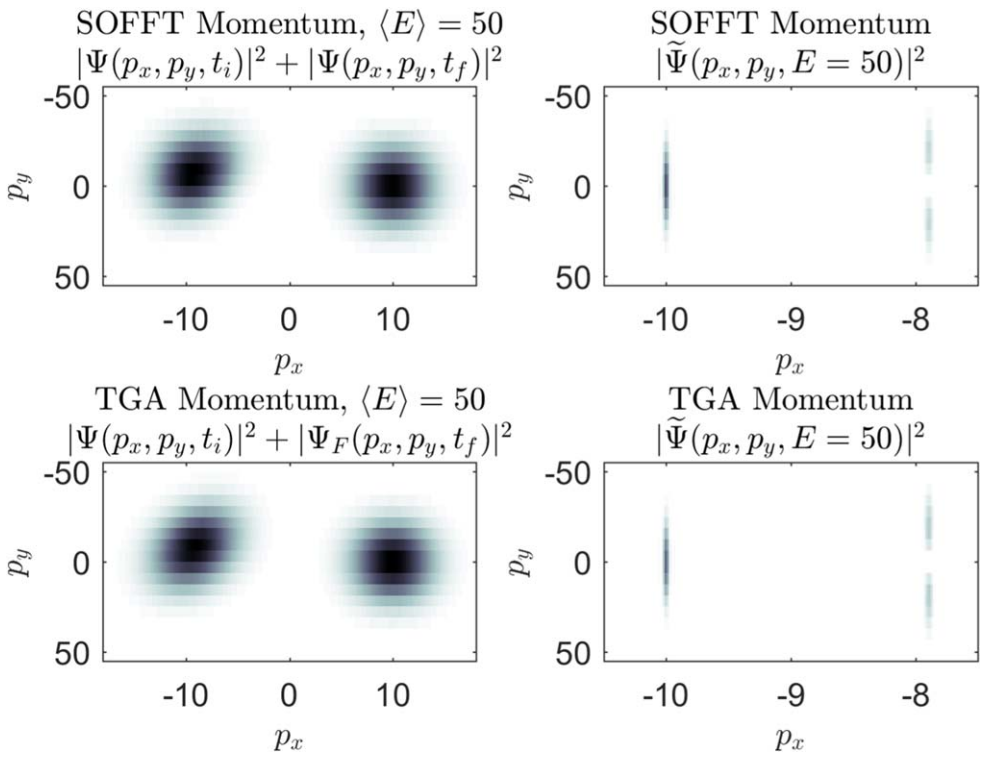

Figure 7. SOFFT versus TGA momentum distribution comparison, $E_{\text{scat}} = 50$—the left shows the direct Gaussian wavepacket momenta before and after collision, while ther right shows the magnitude of the momentum-space energy eigenstates for the dynamics. Note on the right the first excited state of the oscillator which causes the splitting of the wavefunction energies.

total run time of $\tau = 6$ (corresponding to an energy resolution of $\Delta E \approx 1$). We compare the results for the split-operator-evolved and thawed Gaussian wavefunction and plot the results in figure 7.

The initial+final momentum distribution plotted on the right is in both cases large Gaussian (or Gaussian-esque) blobs with little discernible structure. By performing the Fourier transform we can see the eigenstate structure emerge naturally; we see the superposition of the incoming plane-wave and ground state oscillator, together with the outgoing state where the first (and, although not discernible to the eye, second) mode of the harmonic oscillator has been excited with finite probability.

We then look at the position space energy Fourier transform of the wavefunction, $\psi(x, y, E)$, as shown in figure 8. We can then integrate over the y-coordinate of this function:

$$\rho_{\text{red}}(x, x, E) = \int |\psi(x, y, E)|^2 \, dy \tag{78}$$

and look at the resulting reduced wavefunction to look at the fringe contrast as a result of the interaction.

Close to the interaction region, there is clear disagreement in the two wavefunctions; this is to be anticipated from the poor overlap of the wavefunction in that region. One feature to note is that near the interaction region the thawed Gaussian has lower probability density than

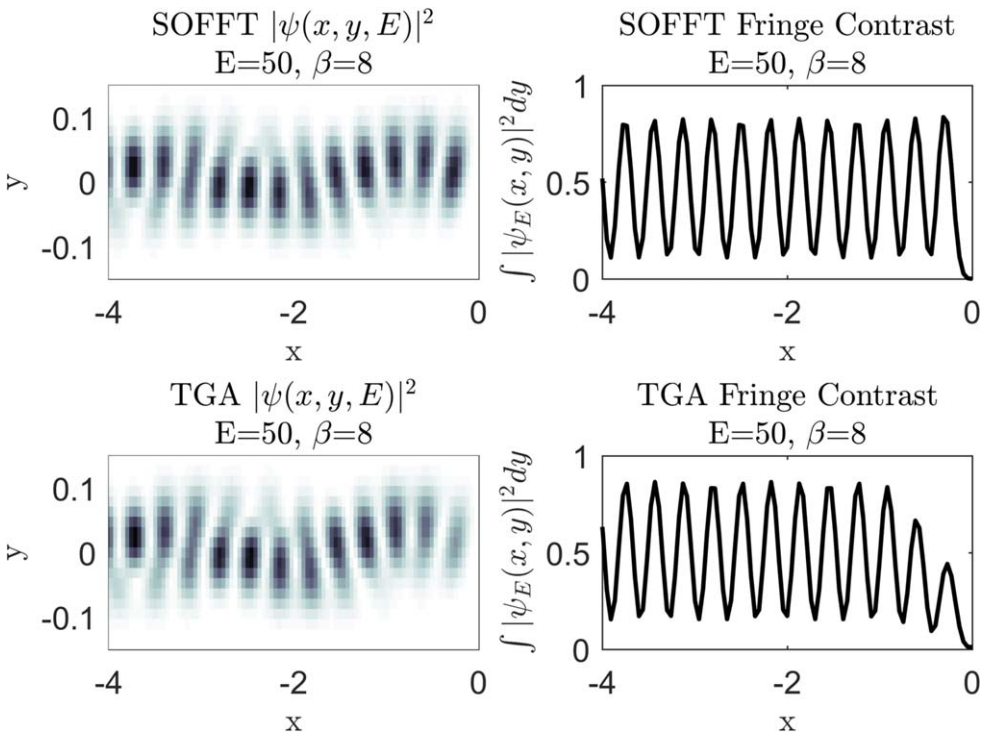

Figure 8. Energy Fourier-transformed wavefunction and fringe contrast—note that the dynamics far from the interaction region are qualitatively similar; however, close to the interaction region the behaviour diverges.

the SOFFT result. This is a result of the non-conservation of energy inherent in the thawed Gaussian approximation (as we are effectively evolving a time-dependent potential) and the presence of the wavefunction in the region of large potential acts to shift its energy artificially high. Far away from the interaction region, the two energy-space wavefunctions are very similar and have the expected form of plane wave with diminished fringe contrast.

We then look at the magnitude of the fringe contrast (equivalently $|c_0|$) versus energy, including the forced harmonic oscillator results and exact results (for a hard wall rather than an exponential potential) for comparison:

Both the thawed Gaussian and split-operator methods retain the basic behaviour of the exact solution; both methods struggle a bit for $E \approx 2$ and $E \approx 20$ due to the fundamental abrupt change in behaviour. For intermediate energies the thawed Gaussian performs relatively poorly for the parameter α_0 chosen; it overestimates the excitation of the harmonic oscillator but generally indicates the character of the result. In particular, note in figure 9 the drops in fringe contrast at the integer multiples of the harmonic oscillator frequency (resonances). As in the hard wall solution, the 'classical' forced harmonic oscillator excitation fundamentally diverges from the quantum result at low energy and underestimates the behaviour at high energy. The exact hard-wall solution matches the tabulated split-operator results, but slightly diverges at higher energies due to the inclusion other energies in the numerical wavefunction due to the finite energy spread of the Fourier-transformed wavefunction.

We can get further insight by altering the exponential parameter β. This changes the stiffness of the parameter, shifting the interaction from a gentle collision to an impulsive hard

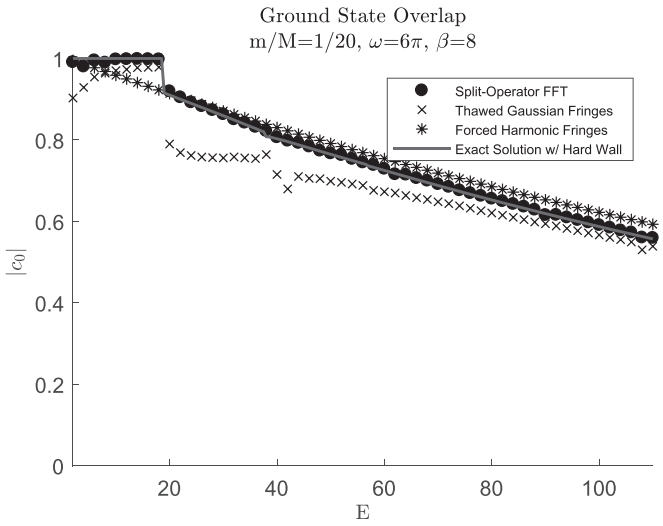

Figure 9. Ground state overlap versus energy—the thawed Gaussian method, while flawed, retains much of the qualitative behaviour of the exact dynamics (notably, the dips at integer multiples of the harmonic oscillator energy) . We include, for reference, the exact analytical solution with the fixed infinite hard wall interaction.

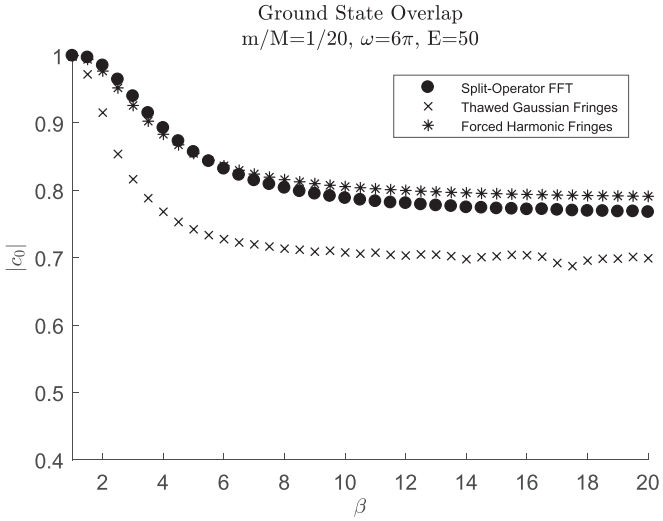

Figure 10. Ground state overlap versus exponential steepness β .

wall. We show the results for the split-operator, thawed Gaussian and forced harmonic oscillator methods in figure 10.

While the three different methods produce different raw values they all reveal the same fundamental behaviour: the stiffest potentials asymptote to a fixed value of excitation. For a softer, gentler collision, we produce small, but still finite, excitation of the harmonic oscillator despite the total change of momentum from $p_x \rightarrow -p_x$, as alluded to in a recent work on Helium scattering by the authors [35].

5. Conclusion

As Richard Feynman [16] noted, 'the exact analysis of real physical problems is usually quite complicated, and any particular situation may be too complicated to analyse directly by solving the differential equation.' Similar to how the field equations in electromagnetics are commonly reduced to concepts of impedances in order to make sense of and make practical use of the fundamental equations, when studying decoherence the infinite microscopic differential equations representing the bath are reduced to a master equation that encapsulates the collective behaviour and its influence on the system in question. However, restricting oneself to examining only a resistance without considering the effect of two charged particles on each other would be a pedagogical disservice; similarly, there is disservice done by not considering the low-particle limit of the concepts of entanglement and decoherence. The simple model of decoherence that we introduce here is approached and solved analytically and numerically, using both approximate and exact methods, designed to contribute physical intuition and inspire problem solving prowess.

ORCID iDs

Matthew C Schram https://orcid.org/0000-0003-1203-0621

References

[1] Zurek W H 2003 Decoherence, einselection, and the quantum origins of the classical *Rev. Mod. Phys.* **75** 715–75
[2] Palma G M, Suominen K-A and Ekert A K 1996 Quantum computers and dissipation *Proc. R. Soc.* A **452** 567–84
[3] Gallis M 1996 Emergence of classicality via decoherence described by Lindblad operators *Phys. Rev.* A **53** 655–60
[4] Maniscalco S, Piilo J, Intravaia F, Petruccione F and Messina A 2004 Lindblad- and non-Lindblad-type dynamics of a quantum Brownian particle *Phys. Rev.* A **70** 032113
[5] Gamble J K and Lindner J F 2009 Demystifying decoherence and the master equation of quantum brownian motion *Am. J. Phys.* **77** 244–52
[6] Wang W-g, He L and Gong J 2012 Preferred states of decoherence under intermediate system-environment coupling *Phys. Rev. Lett.* **108** 070403
[7] Ingold G-L, Hänggi P and Talkner P 2009 Specific heat anomalies of open quantum systems *Phys. Rev.* E **79** 061105
[8] Clarke M L 2013 Emerging interpretations of quantum mechanics and recent progress in quantum measurement *Eur. J. Phys.* **35** 015021
[9] Kardar M 2007 *Statistical Physics of Particles* (Cambridge: Cambridge University Press)
[10] Blum K 2010 *Density Matrix Theory and Applications* (New York: Plenum)
[11] Economou E N 2006 *Greenas Functions in Quantum Physics* 3rd edn (Berlin: Springer)
[12] Greenberger D M 1983 The neutron interferometer as a device for illustrating the strange behavior of quantum systems *Rev. Mod. Phys.* **55** 875–905
[13] Griffiths D 2016 *Introduction to Quantum Mechanics* (Cambridge: Cambridge University Press)
[14] Klauder J and Sudarshan E 1968 Fundamentals of quantum optics *The Mathematical Physics Monographs Series* (New York: Benjamin)
[15] Schrodinger E 1926 Der stetige Übergang von der mikro- zur makromechanik *Naturwissenschaften* **14** 664–6
[16] Feynman R, Leighton R and Sands M 1964 *The Feyman Lectures on Physics* (Reading, MA: Addison-Wesley)
[17] Kincaid J, McLelland K and Zwolak M 2016 Measurement-induced decoherence and information in double-slit interference *Am. J. Phys.* **84** 522–30

[18] Stern A, Aharonov Y and Imry Y 1990 Phase uncertainty and loss of interference: a general picture *Phys. Rev.* A **41** 3436–48
[19] Lerner L 2017 A demonstration of decoherence for beginners *Am. J. Phys.* **85** 870–2
[20] Villars C N 1984 Observables, states and measurements in quantum physics *Eur. J. Phys.* **5** 177–83
[21] Sakurai J J 1994 *Modern Quantum Mechanics* Revised edn (Reading, MA: Addison-Wesley)
[22] Heller E J 1975 Time-dependent approach to semiclassical dynamics *J. Chem. Phys.* **62** 1544
[23] Tannor D J 2007 *Introduction to Quantum Mechanics: A Time-Dependent Perspective* 1st edn (Mill Valley, CA: University Science Books)
[24] Strang G 1994 Wavelets *Am. Sci.* **82** 250–5 (https://www.jstor.org/stable/29775194)
[25] Higgins R J 1976 Fast fourier transform: an introduction with some minicomputer experiments *Am. J. Phys.* **44** 766–73
[26] The Mathworks, Inc., Natick, Massachusetts, MATLAB version 8.5.0.197 613 (R2015a), 2015
[27] Husimi K 1953 Miscellanea in elementary quantum mechanics: ii. *Prog. Theor. Phys.* **9** 381–402
[28] Gottfried K and Yan T-M 2003 *Quantum Mechanics: Fundamentals* 2nd edn (Berlin: Springer)
[29] Feynman R P 1950 Mathematical formulation of the quantum theory of electromagnetic interaction *Phys. Rev.* **80** 440–57
[30] Merzbacher E 1998 *Quantum Mechanics* 3rd edn (New York: Wiley)
[31] Landau L and Lifshitz E 1976 *Mechanics* 3rd edn (Oxford: Butterworth-Heineman)
[32] Wehrle M, Šulc M and Vaníček J 2014 On-the-fly *ab initio* semiclassical dynamics: identifying degrees of freedom essential for emission spectra of oligothiophenes *J. Chem. Phys.* **140** 244114
[33] Balasubramanian S 2001 Time-development operator method in quantum mechanics *Am. J. Phys.* **69** 508–11
[34] Blinder S M 1968 Evolution of a gaussian wavepacket *Am. J. Phys.* **36** 525–6
[35] Schram M C and Heller E J 2018 Approach to coherent interference fringes in helium-surface scattering *Phys. Rev.* A **98** 022137